Case Studies in Thermal Engineering 4 (2014) 99–112

Contents lists available at ScienceDirect

Case Studies in Thermal Engineering

journal homepage: www.elsevier.com/locate/csite

Numerical and experimental analysis for exhaust heat exchangers in automobile thermoelectric generators

Shengqiang Bai [a,*], Hongliang Lu [b], Ting Wu [a], Xianglin Yin [a], Xun Shi [c], Lidong Chen [c]

[a] CAS Key Laboratory of Energy Conversion Materials, Shanghai Institute of Ceramics, Chinese Academy of Sciences, Shanghai 200050, China
[b] Shanghai Institute of Special Equipment Inspection and Technical Research, Shanghai 200333, China
[c] State Key Laboratory of High Performance Ceramics and Superfine Microstructure, Shanghai Institute of Ceramics, Chinese Academy of Sciences,
1295 Dingxi Road, Shanghai 200050, China

ARTICLE INFO

Article history:
Received 10 June 2014
Accepted 9 July 2014
Available online 27 July 2014

Keywords:
CFD
Energy recovery
Thermoelectric generator
Automobile exhaust
Heat transfer

ABSTRACT

Ideal heat exchangers recover as much heat as possible from an engine exhaust at the cost of an acceptable pressure drop. They provide primary heat for a thermoelectric generator (TEG), and their capacity and efficiency is dependent on the material, shape, and type of the heat exchanger. Six different exhaust heat exchangers were designed within the same shell, and their computational fluid dynamics (CFD) models were developed to compare heat transfer and pressure drop in typical driving cycles for a vehicle with a 1.2 L gasoline engine. The result showed that the serial plate structure enhanced heat transfer by 7 baffles and transferred the maximum heat of 1737 W. It also produced a maximum pressure drop of 9.7 kPa in a suburban driving cycle. The numerical results for the pipe structure and an empty cavity were verified by experiments. Under the maximum power output condition, only the inclined plate and empty cavity structure undergoes a pressure drop less than 80 kPa, and the largest pressure drop exceeds 190 kPa. In this case, a mechanism with a differential pressure switch is essential to bypass part of the exhaust.

1. Introduction

Statistics released by the Ministry of Public Security found that there were more than 240 million vehicles operated in China in the end of 2012; and the annual consumption of vehicle fuel broke 269 million tons according to The 2012 Foreign Oil and Gas Industry Development Report by China Petroleum Economic Institute of Technology. For vehicles with internal combustion engine, approximately 40% of the fuel's chemical energy is wasted as exhaust gas [1], the amount of waste heat in terms of the 2012's fuel consumption is extraordinarily large at 107.6 million tons of vehicle fuel. If only a part or even a

* Corresponding author. Tel.: +86 21 69987153; fax: +86 21 69987781.
E-mail address: bsq@mail.sic.ac.cn (S. Bai).

http://dx.doi.org/10.1016/j.csite.2014.07.003

Nomenclature

b_e	fuel consumption rate, g/(kW h)
h	enthalpy, kJ/kg
j	intake efficiency factor
L_0	mass of required air when 1 kg gas combusts completely, kg/kg
S_E	an optional volumetric heat source, W/m^3
P_e	effective engine power, kW
$\nabla(U\cdot\tau)$	the vicious work, W
U_S	the solid velocity, if specified, m/s
US_M	work due to external momentum sources, W

Subscripts

m	moment
s	velocity
Tot	total

Greek letters

α	surplus factor of air more than complete combustion
λ	thermal conductivity of the solid
ρ	density
τ	stress tensor

minor amount of the large waste heat could be recovered and converted into electricity, a great sum of heat would be saved and the system efficiency of the vehicle would increase substantially.

Various thermodynamic cycles have been proposed and studied for low-grade waste heat recovery. An absorption cooling cycle in hybrid and electric vehicles transfers waste heat from the battery pack and exhaust gases into the boiler of ejector for cabin cooling [2]. The organic Rankine cycle system possesses the capability to convert low grade heat sources into electricity [3]. An open steam power cycle (open Rankine cycle) has a greater waste heat recovery efficiency than other Rankine steam cycles [4]. A combined thermoelectric generator and organic Rankine cycle was proposed to increase the system performance of exhaust heat recovery [5]. Usually, the disadvantage of these cycles is the secondary fluid circuit composed of a pump, an evaporator, an expander and a condenser; the circuit increases vehicle weight and mechanical complexity and reduces available volume. Based on the Seebeck effect, the thermoelectric generator system takes the advantage of no moving parts, silent operation, and very reliable, therefore better suited waste heat recovery from automobile exhausts than the above cycles [6].

With the development of advanced thermoelectric materials, the direct energy conversion of waste heat into electric power has become a popular research topic [7] and one of the biggest challenges for this application in automobile is the exhaust heat exchanger: it must meet requirements for an efficient TE generator and, at the same time, not impede the operation of the vehicle. According to fuel consumption data for one vehicle [8] and related measurement methods [9], an automobile exhaust system is low in the time-averaged mass flow rate: 14.4 g/s for a vehicle with a 1.2 L gasoline engine under a suburban driving cycle and less than 1.2 kJ/(kg °C) in specific heat. The low mass flow rate and limited allowable pressure drop of an automobile exhaust gas represent a double challenge to a design of the exhaust heat exchanger of energy recovery system.

The material, the shape and type of an exhaust heat exchanger have been studied previously. Two shapes of exhaust heat exchangers are generally used for an automobile exhaust TEGs: box and cylinder shells with internal fins. Early in the 1988, Birkholz et al. [10] proposed a 300 mm × 300 mm × 500 mm rectangular structure with internal fins made of the Hastelloy X alloy for the Porsche 944 engine. The box's height was high enough to prevent engine power deterioration. Bass et al. [11] designed a hexagonal cylinder that was 470 mm in length and 220 mm in diameter with a center hollow displacement conic heat-diffuser. Ikoma et al. developed a 160 mm × 40 mm × 455 mm rectangular box using SUS304 stainless steel [12]. Fins with different area ratios (0.92,1.21,1.65,1.99) were set inside the inner shell, parallel to the gas flow, to transfer more heat [13,14]. Thacher et al. [15] used a rectangular 1018 carbon steel compact heat exchanger with offset strip fins for a 1999 GMC Sierra pick-up truck. Crane et al. [16] employed a cylindrical design with internal folded fins made of stainless steel–clad copper. As for the exhaust heat exchanger optimization and theoretical analyses, CFD simulations and geometry improvements were conducted to enhance turbulence and heat transfer. Crane et al. [17] used hot water as a heat source and air as a heat sink to simulate an exhaust thermoelectric generator. Martinez et al. [18,19] calculated the thermal resistance and pressure drop for a heat exchanger and used computational fluid dynamics to optimize the thermoelectric generator for a domestic gas boiler. Ming Pan [20] conducted thermal and hydraulic calculations on the intensification combinations. Gou [21] studied the dynamic characteristics of heat reservoir and heat sink for thermoelectric generators. Sun [22] conducted optimal design considering the fluctuation of industrial waste heat. Such numerous types of materials, structure parameters and operating conditions involved in the energy transformation and transfer process make it difficult to evaluate which type of the heat exchanger is the best or most fit for automobile exhaust TEG. CFD is a powerful tool that is capable of comparing several heat exchangers under the same boundary conditions [23,24]. One or multiple candidates may be found to further optimize a specific automobile type under a specific driving cycle, and this is one important approach to studying automobile exhaust TEGs.

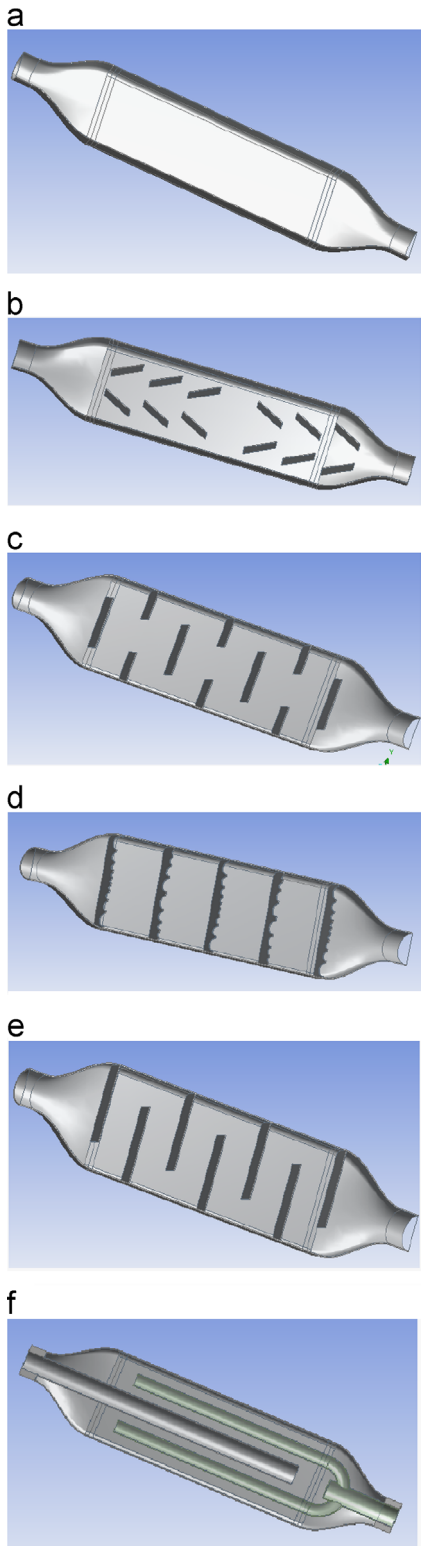

Fig. 1. Six internal structures. (a) Empty cavity, (b) inclined plate, (c) parallel plate structure, (d) separate plate with holes, (e) serial plate structure and (f) pipe structure.

The present work reviews existing exhaust heat exchangers and proposes several internal structures: an inclined plate, a parallel plate structure, a separate plate with holes, a serial plate structure, and a novel pipe structure. CFD models were developed with solid domains, liquid domains and fluid solid interfaces to compare the heat transfer and pressure drop for the 6 structures under the same working conditions. The numerical results suggest that the serial plate structure offers the highest heat transfer, while its pressure drop is excessively large under the maximum power output condition.

2. Simulation analyses

2.1. Six internal structures of exhaust heat exchangers

For the purpose of comparison, 6 structures were made with the same dimensions, with a shell of 280 mm × 110 mm × 30 mm with the inlet and outlet of 40 mm in diameter for 5 of the structures. The pipe structure was reduced to 26 mm in diameter because the shell body was 30 mm thick. At both ends of the box, there were gradual enlargements and contractions of approximately 90 mm in length to buffer and distribute exhaust flow. Each exhaust exchanger had a different internal structure: an inclined plate, a parallel plate structure, a separate plate with holes, a serial plate structure, and a novel pipe structure, as shown in Fig. 1.

To reduce mesh quantity and promote the robustness and precision, only half of the whole body was used, and the model was obtained using a symmetrical plane. The number of mesh elements increased with complexity. An empty cavity structure had the fewest elements with 436,087, and the separate plate with holes structure had the most elements with 745,390, 71% more than the former due to its 5 complex thin fins with different holes.

The quality and quantity of a mesh for a certain physical body determines the robustness, accuracy and scale of the simulation computation. Skewness is one of the primary quality measures for a mesh. A value of skewness in the range of 0.25–0.5 indicates that the corresponding mesh quality is good. The mesh quality for the 6 structures was in the range given in Table 1. The pipe structure, with the skewness 0.3193, had the worst mesh quality.

2.2. Simulation operating condition

The exhaust mass flow, exhaust temperature and hot side temperature of thermoelectric generators are three key variables, and they depend on the automotive configuration, operation conditions and available thermoelectric materials.

2.2.1. Exhaust mass flow rate

The mass flow rate of the exhaust gas is the most important parameter for determining the capacity of an automotive exhaust thermoelectric generator, and it depends on operating conditions and engine configuration. The tested passenger car was configured with a 1.2 L gasoline engine, as shown in Table 2.

The field test fuel consumption data for the tested vehicle are provided in Table 3 by the Ministry of Industry and Information Technology of the People's Republic of China according to the ruled measurement methods by GB/T 19233-2008. The corresponding time-averaged exhaust mass flow rate was obtained by Eq. (1) [25].

$$Q_m = P_e b_e (L_0 \alpha j + 1) \tag{1}$$

Table 1
Mesh of each scheme.

Scheme	Empty cavity	Inclined plate	Parallel plate	Separate plate with holes	Serial plate	Pipe structure
Nodes	133,549	136,411	139,290	226,954	142,281	246,085
Elements	436,087	439,420	445,264	745,390	452,802	671,203
Skewness	0.2613	0.2697	0.2796	0.2907	0.2832	0.3193

Table 2
Vehicle configuration.

Engine type	P-TEC, LMU
Transmission	MT-5
Displacement (cm^3)	1206
Cylinders	4
Valves	16
Maximum power (kW/rpm)	63/6000
Maximum torque (N m/rpm)	108/4000
Injection system	Electric-controlled injection

Table 3
Fuel consumption.

Driving cycle	Fuel consumption (L/100 km)	Time-averaged exhaust mass flow rate (g/s)
Urban	6.7	5.7
Suburban	5.1	14.4
Overall	5.7	8.53
Maximum power output	–	80.14

Table 4
Operating condition.

Driving cycle	Mass flow rate of exhaust (g/s)	Hot side temperature of generator (K)	Exhaust temperature (K)
Urban	5.7	423.15	573.15
Suburban	14.4	473.15	673.15
Maximum power output	80.1	423.15	873.15

2.2.2. Exhaust state

Exhaust is a mixture of multiple compositions and is thermodynamically similar to air. Exhaust is approximately 300–500 kPa in pressure and 500–700 °C in temperature when discharged from the engine cylinder [26]. After passing through the catalytic converter and several connecting pipes, the pressure drop nears the atmospheric pressure and the temperature decreases to 300–600 °C because of local and frictional losses and heat leaks. The initial state of the exhaust gas at the inlet is important as a heat source for two reasons: first, it determines the maximum available heat in reference to the atmosphere state; second, it determines the upper temperature limit to which the TE material is exposed and which it must survive.

2.2.3. Hot side temperature of a thermoelectric generator

The hot side of the thermoelectric generator absorbs heat from the shell and transfers it to the cold side. Its upper temperature limit is subjected to the maximum continued temperature the thermoelectric material can be exposed to, for instance, 150–250 °C is acceptable for Bi_2Te_3. According to the range of the above variables, three typical operation conditions were considered in Table 4: urban and suburban driving cycles and maximum power output.

2.3. Theory and boundary configuration

The total computing domain includes a fluid portion and a solid portion. The temperature field and flow field of interest are obtained by solving a set of mathematical equations with respect to computational fluid and solid domains. Within the fluid domains, the equations of mass, momentum and energy conservation (Eqs. (2)–(4)) are solved to model fluid flow, heat and mass transfer. Only the equation of heat transfer is solved for solid domains (Eq. (5)).

The continuity equation is

$$\frac{\partial \rho}{\partial t} + \nabla \cdot (\rho U) = 0 \tag{2}$$

The momentum equation is

$$\frac{\partial (\rho U)}{\partial t} + \nabla(\rho UU) = -\nabla p + \nabla \tau + S_M \tag{3}$$

The energy equation is

$$\frac{\partial (\rho h_{\text{tot}})}{\partial t} - \frac{\partial p}{\partial t} + \nabla(\rho U h_{\text{tot}}) = \nabla(\lambda \nabla T) + \nabla(U\tau) + US_M + S_E \tag{4}$$

The conservation of energy equation in solid domain is

$$\frac{\partial (\rho h)}{\partial t} + \nabla(\rho U_S h) = \nabla(\lambda \nabla T) + S_E \tag{5}$$

Under the given exhaust pressure and temperature, the speed of sound is 515 m/s, much greater than the real flow velocity, meaning that the fluid model is uncompressible. The viscous model depends on the flow type: laminar flow or

turbulent flow. For the inlet pipe and box cavity, the critical flow velocities are 0.92 m/s and 0.42 m/s, respectively, both of which are much lower than the real velocity. The k-epsilon turbulence model was employed to simulate the exhaust, as it is the industry standard model for many commercial CFD models. This model has been proven to be stable and numerically robust. The fluid material for the exhaust uses a calorically perfect ideal gas because the two are near to one another thermodynamically, and the solid material for shell employs steel.

A general connection technology for the fluid–solid interface was used to connect non-matching grids of the solid domain and fluid domain, such as the exhaust with a shell and the exhaust with a pipe. The fluid–solid interface was also modified to compute heat transfer from the exhaust to the shell after the energy equation was applied to the exhaust domain and the shell domain.

3. Result and discussion

In this section, 6 structures are compared regarding heat transfer and pressure drop under urban driving, suburban driving and maximum power output. Their temperature fields and the flow fields were analyzed under the suburban driving cycle.

3.1. Performance comparison under typical operating conditions

The amount of heat extracted from the exhaust was equal to the enthalpy difference of the exhaust at the inlet and the outlet multiplied by the mass flow rate under the given boundary condition. The 6 structures differed in the heat transfer rate (Figs. 2 and 3) and can be ordered by the decreasing heat transfer as follows: serial plate structure, separate plate with holes, parallel plate structure, pipe structure, inclined plate structure and empty cavity. This order was the same under all 3 of the typical driving cycles. The serial plate structure had the maximum heat transfer rate of 597 W, 1737 W and 14971 W, which were 3.55, 3.73 and 2.96 times the empty cavity structure for the urban driving cycle, the suburban driving cycle and the maximum power output, respectively. For each structure, the heat transfer rate increased from 100% under an urban cycle to approximately 280% under a suburban cycle and to approximately 2400% under the maximum power output as the exhaust mass flow rate rose to 250% and to 1400%.

In response to the heat transfer rate, the pressure drop due to the heat exchanger at the exhaust side was the static pressure difference of the exhaust at the inlet and outlet. The pressure drops for the 6 structures also differed from one another (Figs. 2

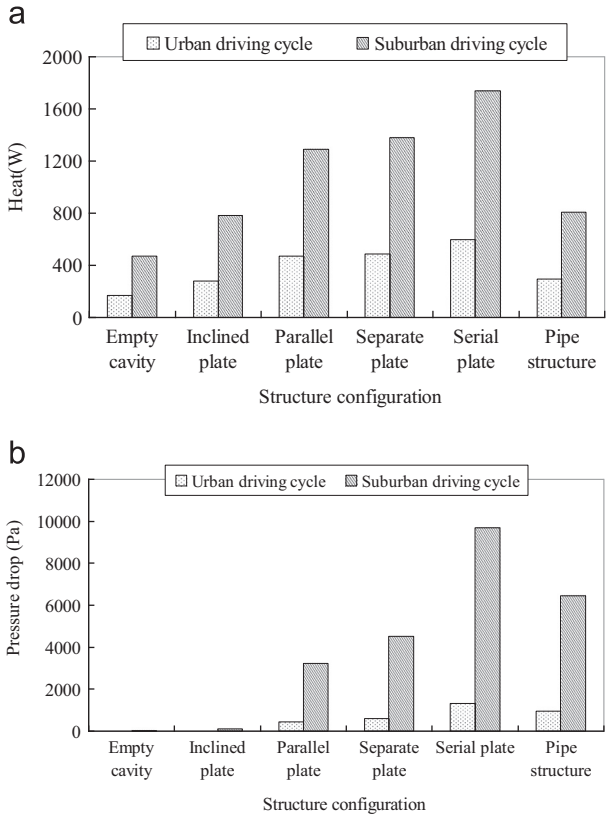

Fig. 2. Performance comparison under urban and suburban driving cycles. (a) Heat transfer rate and (b) pressure drop.

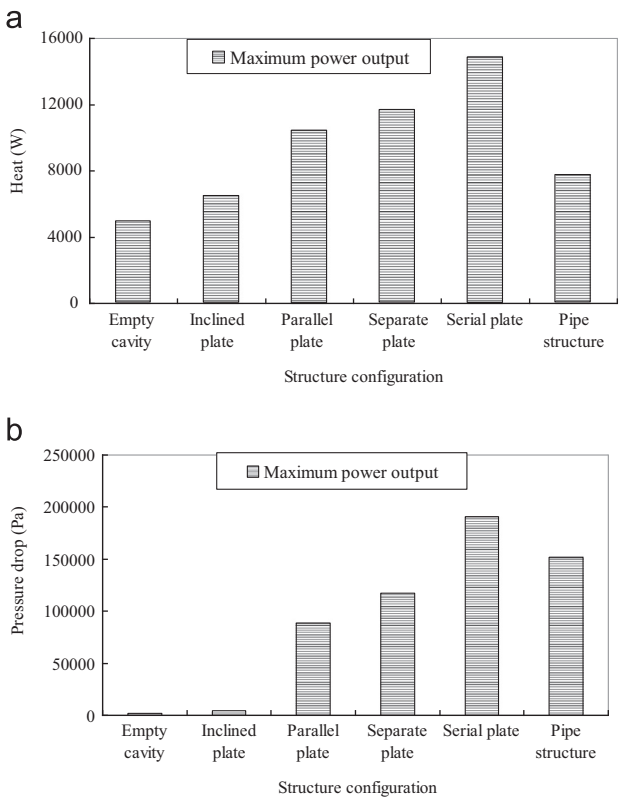

Fig. 3. Performance comparison under maximum power output. (a) Heat transfer rate and (b) pressure drop.

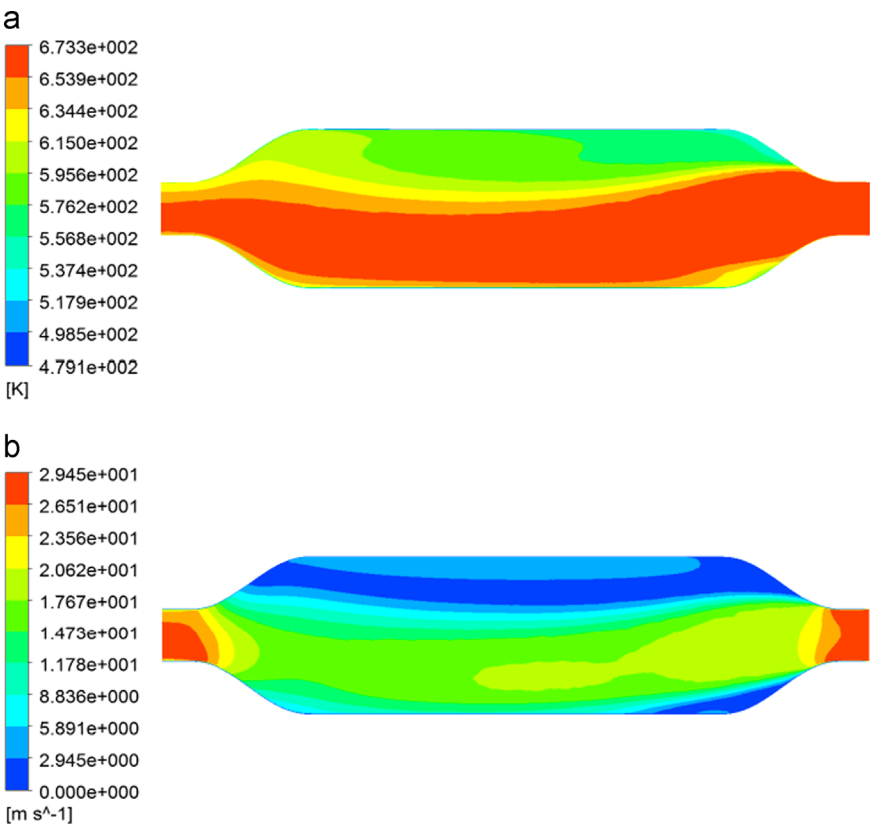

Fig. 4. Physical distribution in an empty cavity. (a) Temperature field and (b) velocity field.

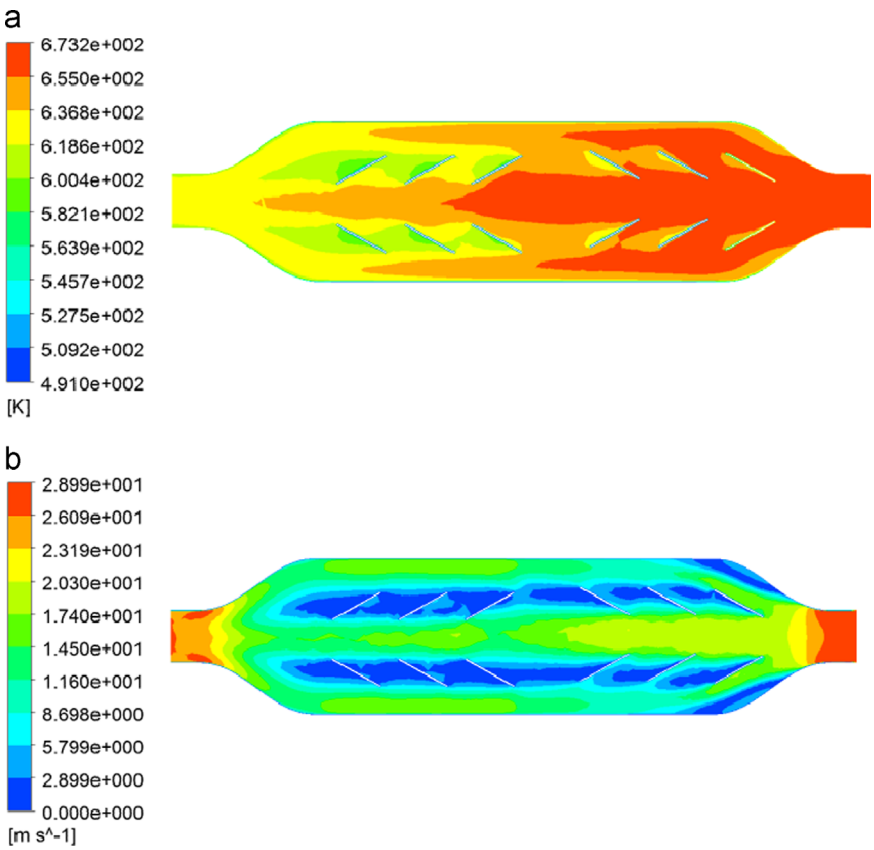

Fig. 5. Physical distribution for a shell with inclined plates. (a) Temperature field and (b) velocity field.

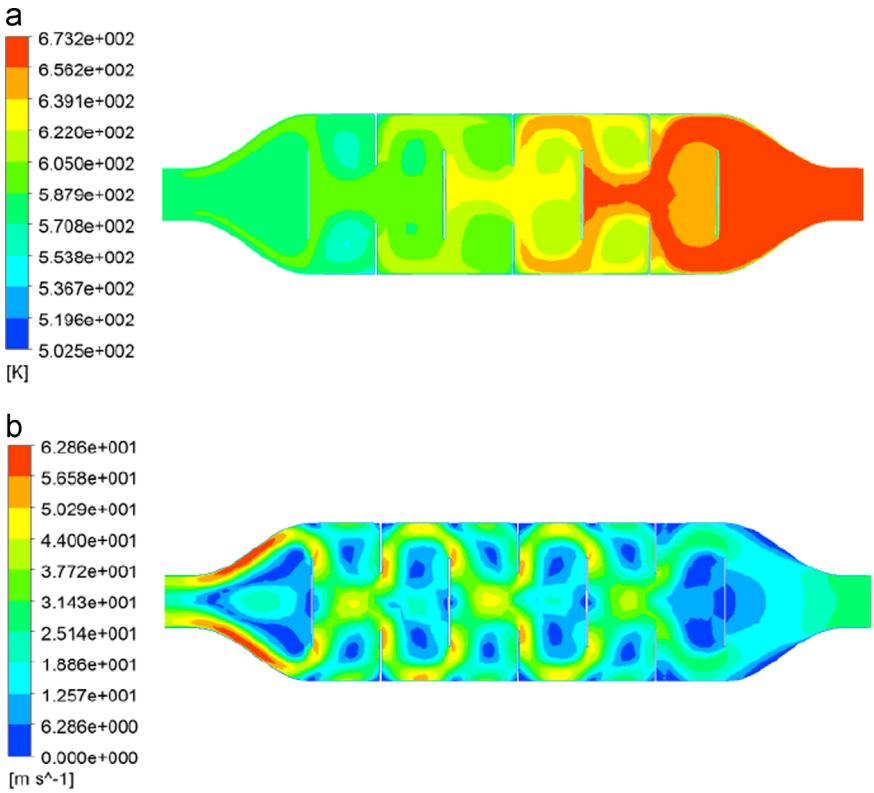

Fig. 6. Physical distribution of a shell with parallel plates. (a) Temperature field and (b) velocity field.

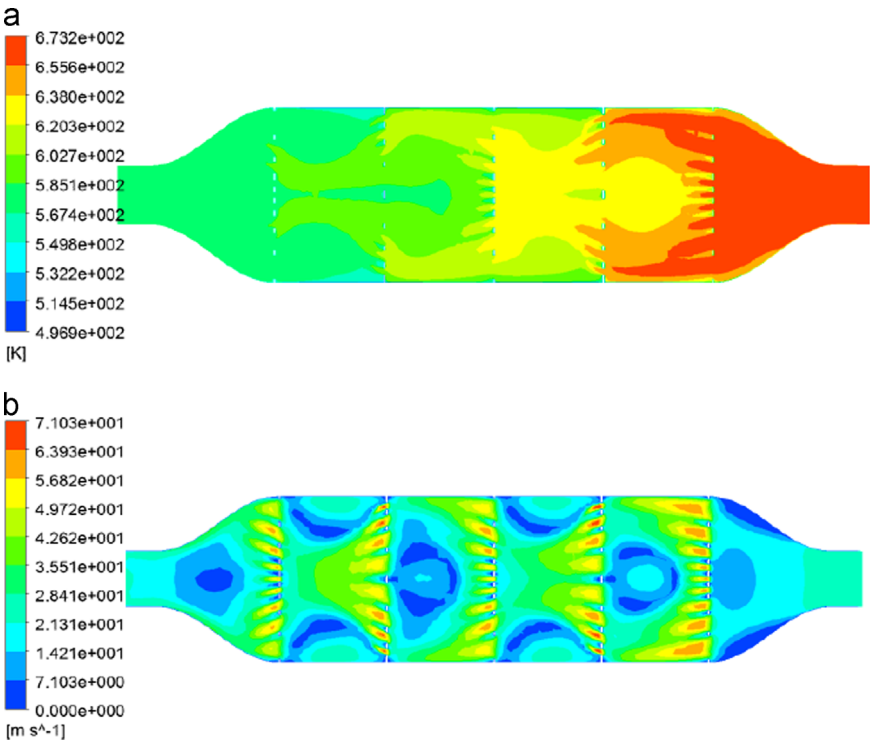

Fig. 7. Physical distribution of a shell with separate plates with holes. (a) Temperature field and (b) velocity field.

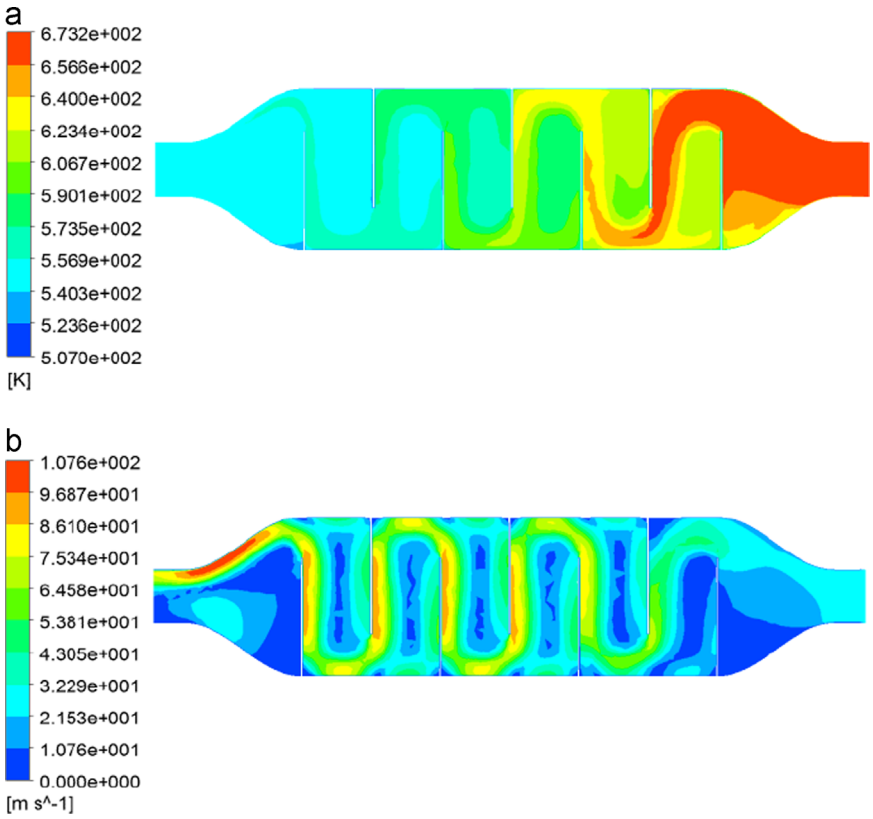

Fig. 8. Physical distribution of a shell with a series of plates. (a) Temperature field and (b) velocity field.

and 3). Under all 3 of the typical operating conditions, the structures' decreasing order of the pressure drop was the same as for the heat transfer: serial plate structure, pipe structure, separate plate with holes, parallel plate structure, inclined plate structure and empty cavity. The serial plate structure had maximum pressure drops of 1.3 kPa, 9.7 kPa and 190.7 kPa, which are 532, 305 and 99 times of empty cavity structure under an urban driving cycle, suburban driving cycle and maximum power output, respectively. This result corresponds to the maximum heat transfer rate among the six structures.

There are two important points to note: first, under the maximum power output condition, if the pressure drops for the serial plate structure, pipe structure, separate plate with holes and parallel plate structure are all greater than 80 kPa, the automobile engine may fail to function or even shutdown if the bypass mechanism is not available. This high pressure drop was also verified by the experiment conducted by Lagrandeur et al. reporting approximately 60 kPa of backpressure through the BMW X6 exhaust component [27]. Therefore, a bypass mechanism with a differential pressure switch is necessary for the engine's stability and reliability. Second, the pipe structure was an exception, as it had the 2nd largest pressure drop but the 4th largest heat transfer rate. In other words, this structure extracted a lower heat per unit pressure drop than the other structures. Third, a larger heat transfer rate usually corresponds to a larger pressure drop for agiven heat exchanger; it provides an upper limit at which to maintain turbulence for increased heat flow until a desirable pressure drop is reached.

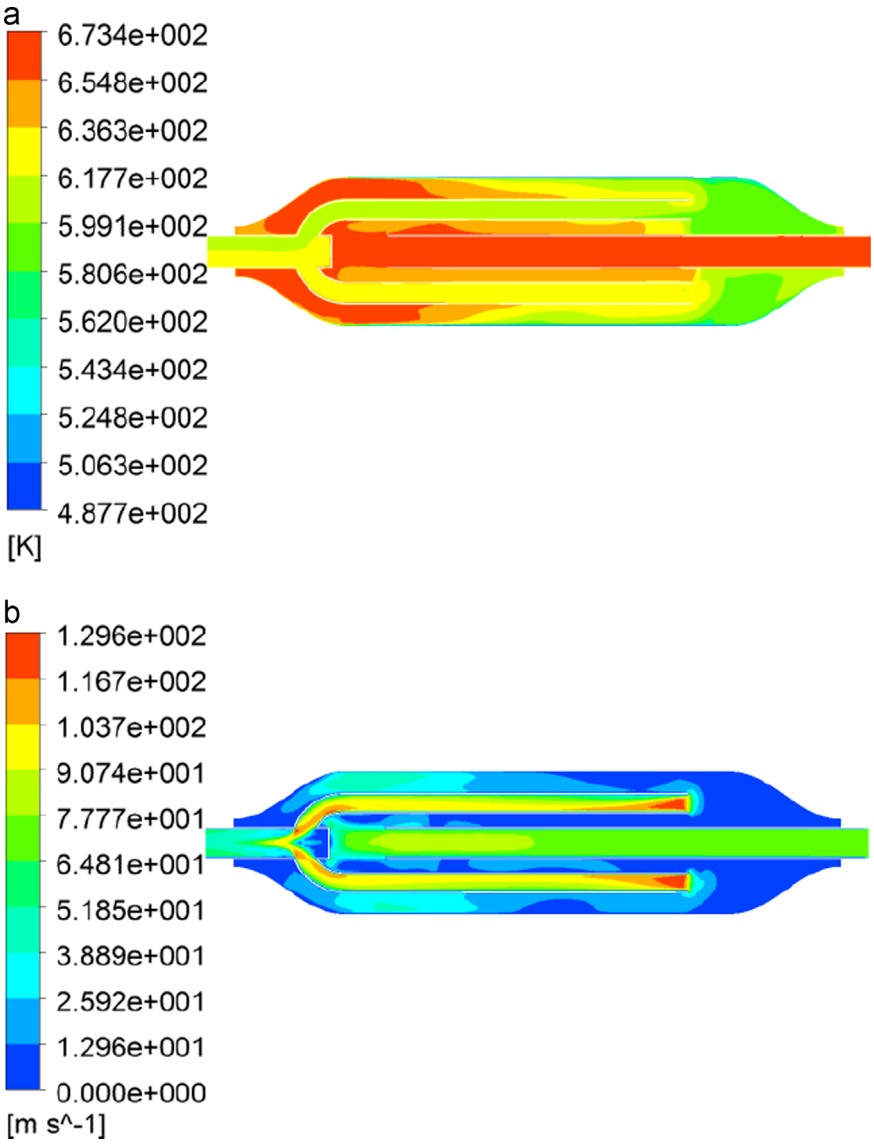

Fig. 9. Physical distribution of a shell with a pipe structure. (a) Temperature field and (b) velocity field.

3.2. Temperature field and velocity field analysis

A different thermal performance and aerodynamics originated from the temperature field and the velocity field of heat exchangers. It was necessary to analyze the physical field of the 6 structures under the same suburban driving cycle. A symmetrical plane along the thickness of the shell was generated to obtain the temperature field and the velocity field of the exhaust.

For the empty cavity, the exhaust expanded gradually at the inlet because it entered the body and left the shell wall with almost the same main flow area, as shown in Fig. 4. In the absence of any structure or fin, some eddies with low temperature and low velocity appeared in the upper side of the empty cavity the most of the hot exhaust left directly from the structure. Only a small amount of heat, 466 W, was transferred to the wall, and the pressure drop was as small as 32 Pa. Compared with the empty cavity, the presence of an inclined fin, as shown in Fig. 5, destroyed the large eddy and allowed the hot exhaust to disperse and collide with walls. Consequently, the heat transfer increased by approximately 67% to 779 W, while the pressure drop increased to 96 Pa.

To further enhance the turbulence and heat transfer, the parallel plate structure, separate plate with holes, and serial plate structure were proposed together. Figs. 6–9 show that the different internal structures all increased heat transfer;

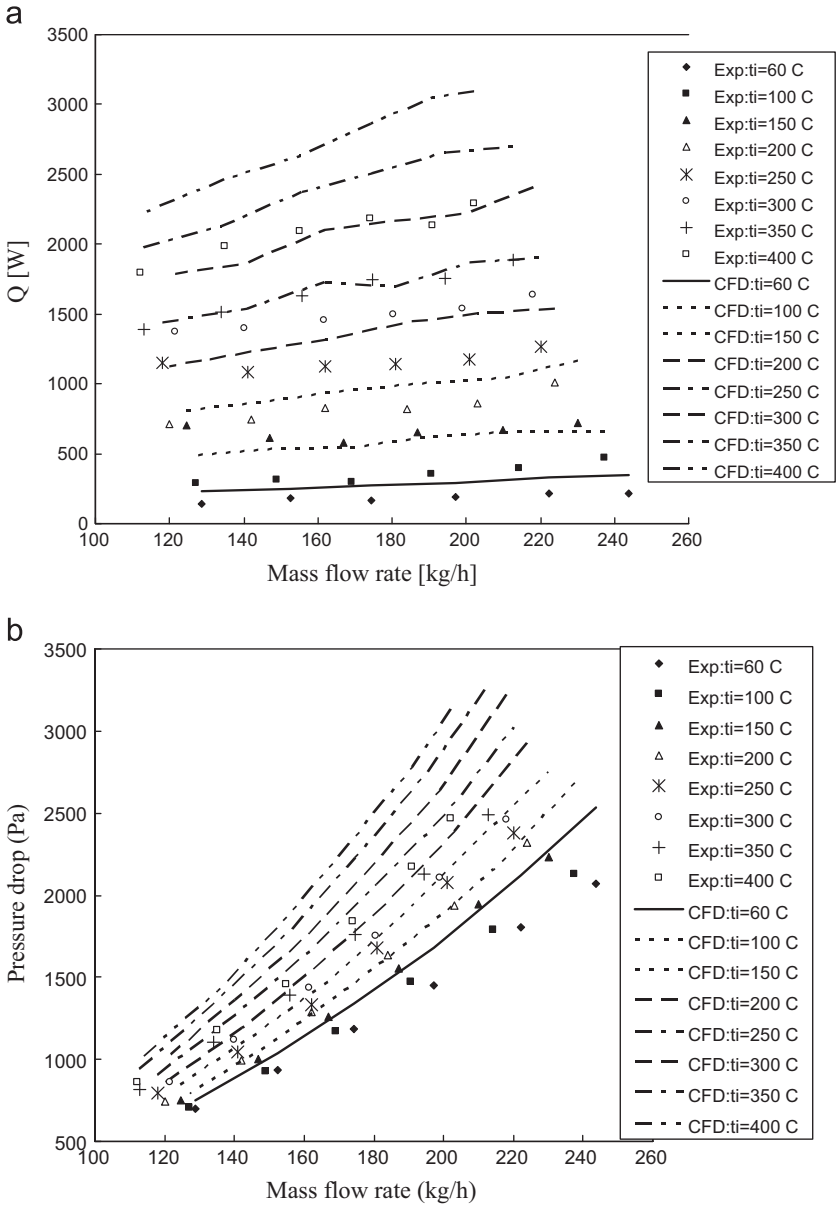

Fig. 10. Numerical and experimental results for the pipe structure. (a) Heat and (b) pressure drop.

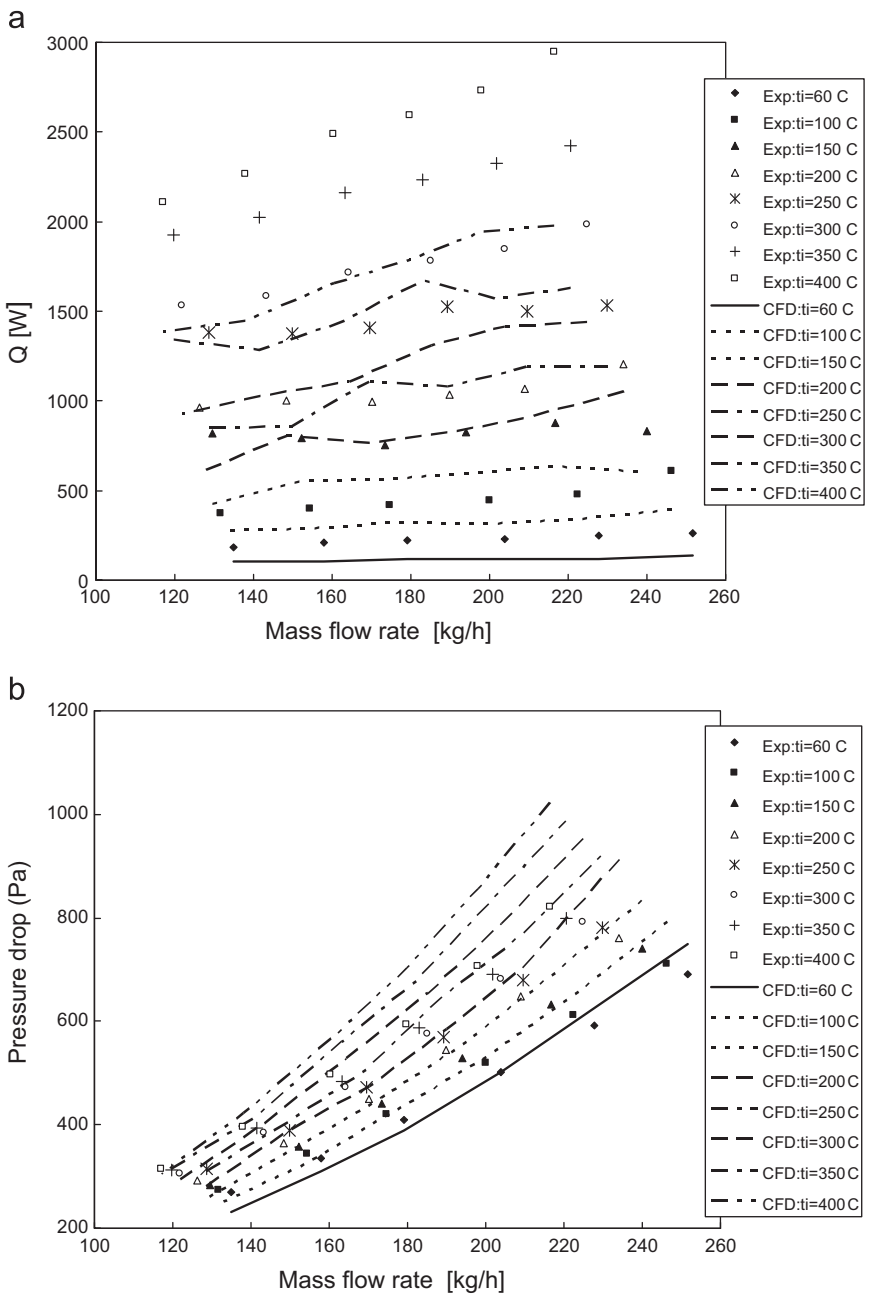

Fig. 11. Numerical and experimental results for the empty cavity. (a) Heat and (b) pressure drop.

meanwhile, the exhaust released heat and gradually became cooler. Several specific areas between two adjacent baffles, at nearly equal temperatures, were provided as hot sources for thermoelectric modules, which are important for the thermoelectric generator. The serial plate structure forced exhaust to flow back and forth using 7 baffles, enhanced the heat transfer with the shell wall and had the maximum heat transfer rate at 1737 W, which was 35% and 26% greater than the parallel plate structure and the separate plate with holes, respectively. The serial plate structure also had a maximum pressure drop of 9.6 kPa among the three, 200% and 115% more than parallel and separate plate structures, respectively.

As for the pipe structure, the exhaust flowed out of the main inlet at the outlet side of the body and diffused until the end area of the main outlet opposite to the outlet of the inlet. There, it reflected and flowed into the two outlet pipes, as shown in Fig. 9. The temperature field was relatively uniform as a whole; however, it released the heat of 805 W, just 46.3% of the serial plate total, while its pressure drop was 6.5 kPa, 66.8% of that of the serial plate. The sudden enlargements and contractions of the inlet or outlets produced a larger pressure drop than in other structures.

4. Comparison of the CFD simulation with experimental results

To validate the CFD models, two heat exchangers were fabricated with the same shell dimensions of 670 mm × 360 mm × 81 mm: One was pipe structure and the other was empty cavity as in the Fig. 1, but a gradual transition from the inlet and the outlet to the body of the heat exchanger was modified into a direct connection.

The experimental setup included K-type thermocouples, a stainless V-cone flow meter with temperature and pressure compensation, a differential pressure transmitter, the pressure transducer and an industrial heat fan to provide hot air that simulated an automobile exhaust. The differential pressure transmitter was set to test the fluid's pressure drop through the exhaust heat exchanger. Hot air at 60–400 °C and a different velocity other than the typical driving cycles was fed into the heat exchangers. The heat exchanger was exposed to the ambient of 22 °C, and the heat extracted from the hot air was equal to the mass flow rate multiplied by the enthalpy difference from the inlet to the outlet. Experiment details were given in [28].

The boundary conditions in CFD were the same as in the experiment: inlet temperature and inlet mass flow rate, but the coefficient of convective heat transfer was set to 15 W/(m^2 °C) in consideration of a radiant heat transfer. In Figs. 10 and 11 the numerical and experimental results are shown at 48 operating points with different temperatures and pressures. For the empty cavity, the averaged relative error was 6.96% between the numerical and experimental pressure drop, and it was 31.57% between the numerical and experimental heat transferred. While for the pipe structure, the numerical result overestimated the experimental result, the averaged relative error was 20.95% for the pressure drop and 49.8% for the heat transferred. Obviously, the relative error was small for the low inlet temperature and small mass flow rate; it rose with the increasing inlet temperature and mass flow rate.

5. Conclusion

CFD models with a solid domain, liquid domain and fluid–solid interfaces were developed for 6 exhaust heat exchangers to simulate the temperature field and the velocity field. Under 3 typical driving cycles, the descending order of pressure drop for 5 of the structures is the same as that for the descending magnitude of the heat transfer rate: serial plate structure, separate plate with holes, parallel plate structure, inclined plate structure and empty cavity. Among the 6 heat exchangers, the pipe structure has the 2nd greatest pressure drop and the 4th greatest heat transfer rate.

The serial plate structure forced the exhaust to flow back and forth by 7 baffles, enhanced the heat transfer with the shell wall and had the maximum heat transfer rate of all the structures, at 1737 W. This rate was 35% and 26% greater than the parallel plate structure and the separate plate with holes, respectively. The serial plate also had a maximum pressure drop of 9.7 kPa, 200% and 115% more than the parallel and separate plates, respectively. The pipe structure released the heat of 805 W, 46.3% of the serial plate, with a pressure drop of 6.5 kPa, 66.8% of the serial plate. Under the maximum power output condition, only the inclined plate and the empty cavity structure had pressure drops less than 80 kPa. The largest pressure drop exceeded 190 kPa. The bypass mechanism with a differential pressure switch is necessary for the engine's stability and reliability in such cases.

Acknowledgments

The authors would like to thank Prof. Ctirad Uher (University of Michigan) for language polish. This work was supported by the National Basic Research Program of China, No. 2013CB632504, the International S&T Cooperation Program of China, No. 2011DFB60150, and the National Natural Science Foundation of China, No. 51102260.

References

[1] Yu C, Chau KT. Energy Convers Manag 2009;50:1506–12.
[2] Javani N, Dincer I, Naterer GF. Energy 2012;46:109–16.
[3] Wang D, Ling X, Peng H, Liu L, Tao L. Energy 2013;50:343–52.
[4] Fu J, Liu J, Ren C, Wang L, Deng B, Xu Z. Energy 2012;44:544–54.
[5] Shu G, Zhao J, Tian H, Liang X, Wei H. Energy 2012;45:806–16.
[6] Yang J. In: IEEE proceedings of the 24th international conference on thermoelectrics; 2005 ISBN 0-7803-9552-2, ISSN 1094-2734, p. 170.
[7] Bell Lon E. Science 2008;321(12):1457–61.
[8] ⟨http://chinaafc.miit.gov.cn/n2050/index.html⟩.
[9] GB/T 19233-2008 Measurement methods of fuel consumption for light-duty vehicles.
[10] Birkholz U, Grob E, Stohre U, Voss K. In: Rao KR, editor. Proceedings of the 7th international conference on thermoelectric energy conversion. Arlington, TX: University of Texas at Arlington; 1988. p. 124–8.
[11] Bass J, Elsner NB, Leavitt A. In: Mathiprakisam B, editor. Proceedings of 13th international conference on thermoelectrics (AIP Conf. Proc., New York); 1995. (p. 295–8.).
[12] Kobayashi M, Ikoma K, Furuya K, Shinohara K, Takao H, Imanishi Y, et al. In: Fleurial J-P, editor. Proceedings of the 15th international conference on thermoelectric; 1996. (p. 373–7.).
[13] Ikoma K, Munekiyo M, Furuya K, Izumi T, Shinohara K. In: Koumoto K, editor. Proceedings of the 17th international conference on thermoelectric; 1998. (p. 464–7.).
[14] Ikoma K, Munekiyo M, Furuya K, Kobayashi M, Kouatsu H, Shinohara K. J Jpn Inst Met 1999;63:1457.
[15] Thacher EF, Helenbrook BT, Karri MA, Richter CJ. J Automob Eng 2007;221:95–107.

[16] Crane DT, Lagrandeur JW. J Electron Mater 2010;39:2142–8.
[17] Crane DT, Jackson GS. Energy Convers Manag 2004;45:1565–82.
[18] Martinez A, Vian JG, Astrain D, Rodriguez A, Berrio I. J Electron Mater 2010;39:1463–8.
[19] Rodríguez A, Vián JG, Astrain D, Martínez A. Energy Convers Manag 2009;50:1236–43.
[20] Pan M, Jamaliniya S, Smith R, Bulatov I, Gough M, Higley T, et al. Energy 2013;57:208–21.
[21] Gou X, Yang S, Xiao H, Ou Q. Energy 2013;52:201–9.
[22] Sun ZX, Gao L, Wang JF, Dai YP. Energy 2012;44:1035–43.
[23] Aslam Bhutta MM, Bashir MH, Kham AR, Ahmad KN, Khan S. Appl Therm Eng 2012;32:1–12.
[24] Giangaspero G, Sciubba E. Energy 2013;58:52–65.
[25] Wang L, Li H, Wan X, Ding H, Jin Z. Energy Eng 2004;3:5–7.
[26] Braess HH, Seiffer U. Handbook of automotive engineering (English version) 2005 (USA: SAE International).
[27] Vehicle technologies office: 2009 advanced combustion R&D annual progress report, ⟨http://energy.gov/eere/vehicles/vehicle-technologies-office-annual-progress-reports⟩, p. 260–3.
[28] Lu H, Wu T, Bai S, Xu K, Huang Y, Gao W, et al. Energy 2013;54:372–7.